Microwave Sensing of Water Quality

KUNYI ZHANG[1], (Student Member, IEEE), REZA K. AMINEH[1], (Senior Member, IEEE), ZIQIAN DONG[1], (Senior Member, IEEE), AND DAVID NADLER[2]

[1]Department of Electrical and Computer Engineering, New York Institute of Technology, New York, NY 10023, USA
[2]Department of Environmental Technology and Sustainability, New York Institute of Technology, Old Westbury, NY 11568, USA

Corresponding author: Reza K. Amineh (rkhalaja@nyit.edu)

ABSTRACT Fine-grained water quality data can facilitate the optimized management of water resources, which have become increasingly scarce due to population growth, increased demand for safe sources of water, and environmental pollutions. There is a pressing need for cost-effective, reliable, re-usable, and autonomous water sensing technologies that can provide accurate real-time water quality measurements. In this paper, we present a microwave sensor array with sensing elements operating at different frequencies in the wide frequency band of 1 GHz to 10 GHz. The use of array allows for collecting more information compared with a single sensor system. The sensor array can be fabricated in a cost-effective way through standard printed circuit board (PCB) technology. Here, it is tested with water solutions of various contaminants and parameter values. The dielectric properties of the water sample with different contaminants and parameter values are measured and provided as well.

INDEX TERMS Complementary split-ring resonators, microwave sensors, water quality sensing.

I. INTRODUCTION

Population growth, urbanization, and climate change have put significant stress on the natural resources related to food, energy and water (FEW) that sustain human livelihood. The sustainable supply of these resources is also impacted by human activities and myriads of factors, such as waste management, changing dietary patterns as well as land use [1]–[5]. In particular, agricultural runoff has been reported to be one of the top pollutants of water sources [6]. As an example, runoff from over fertilization and waste from large farms increase nutrients in natural water sources causing algae outbreaks, which reduces dissolved oxygen in water, causing decline in fishery and disturbing the ecosystem [7], [8]. These factors and the compounded effect of climate change negatively impact surface and ground water quality [9]. To understand the complex interconnection amongst these factors for a more informed decision-making, fine-grain data is needed.

In many cities, current water monitoring systems and stations use a reactive mechanism that measures water quality at limited and fixed locations close to water utilities and water sources [10]. At its current stage, there is not enough

The associate editor coordinating the review of this manuscript and approving it for publication was Xiang Huang.

fine-grained data that can be used to study the dynamic interactions of FEW stressors. Improved data acquisition with autonomous sensor networks for fine-grained data sampling and collection is critical for ensuring urban water sustainability, and better analysis, predictability, and optimization of water resource quality [11]–[13].

To address this need, for the first time, we present a microwave sensor array for water quality testing. Microwave sensing has been utilized over the past decade for a broad area of applications from noise measurement systems [14] and spatial displacement measurement [15] to single-cell viability detection [16] and material characterization [17], [18]. In particular, in [19], a zero-power microwave sensor has been reported for the real-time assessment of water quality based on open-end coaxial sensors.

In microwave sensing and spectroscopy systems, the aim is to characterize the spectral behavior of the materials in a frequency range below 100 GHz. Microwave dielectric spectroscopy can result in a low-cost integrated system for laboratory-on-a-board applications [20]. One important application of this method is material mixture characterization. This is due to the fact that the dispersive properties of mixtures of materials highly depend on their molecular level interactions and charge distributions at microwave frequencies [21]. The sensing part of a microwave material

characterization system can be constructed using either a single resonator [22], [23] or a transmission line (TL) [24]. While the former provides a better sensitivity in a limited frequency bandwidth, the latter is suitable for broadband sensing with reduced sensitivity. For water quality sensing, since different concentrations of various pollutants might have the same dielectric constant at a specific frequency, narrow-band resonator-based methods result in ambiguity in detection. Tackling the tradeoff between the sensitivity and bandwidth to achieve broadband dielectric spectroscopy is challenging.

In this paper, we present an array of five resonator sensors with the elements of the array operating at different frequencies covering a wide bandwidth. This allows for taking the advantage of excellent sensitivity of high quality factor (Q) resonators while, similar to TL approach, collecting information over a wide bandwidth (at multiple frequencies within the band). To implement this task, our presented sensor array is based on metamaterial-inspired resonators. The array is re-usable, cost-effective, and can be mass-produced. The elements of the microwave sensor array operate at different frequencies over a wide frequency spectrum from 1 GHz to 10 GHz. It provides a much richer information for the water samples under test than a single sensor system. Microwave sensor arrays have been used before for mircrofluidic sensing [25] and thin-film sensing [26]. Here, we present the design and evaluation of a microwave sensor arrays for water quality testing.

The frequency range of 1 GHz to 10 GHz has been selected according to the consideration that cost-effective commercial RF/microwave components are available at this range allowing for replacing VNA with inexpensive data acquisition circuitry. Besides, five elements for the sensor array with resonant frequencies, almost uniformly distributed over the above-mentioned band, allows for a thorough study of the water property change within this band. Obviously, having larger number of sensors within this band increases the size of sensor array, renders the design process more complicated, and increases the fabrication cost.

Furthermore, we present the dielectric property measurements of water solutions with various contaminants. To our best knowledge, this is the first attempt that the dielectric properties of water pollutants in microwave regime are reported. The results show the capabilities and limitations of using a microwave sensor array for water quality testing. This paves the way toward the advent of a new generation of water quality sensors which are: 1) compact, (2) cost-effective for mass-production and distribution over vast bodies of water, (3) passive to reduce maintenance cost, (4) re-usable, and (5) flexible for further modification to increase sensitivity and selectivity.

The contributions of the paper include:

1. Presenting the dielectric properties of water solutions with various contaminants and parameter values in microwave regime and over the wide frequency range of 1 GHz to 10 GHz.

2. Using a microwave sensor array to measure the responses to water solutions with various contaminants and parameter values over the wide frequency range of 1 GHz to 10 GHz.

3. Evaluation of sensitivity of the sensor array's elements for major water contaminants and parameter values.

II. MAJOR WATER CONTAMINANTS AND WATER QUALITY PARAMETERS

In this section, we describe some of the major parameters and contaminants commonly considered for water quality testing together with some of their standard levels.

A. NITRATE, PHOSPHATE, AND AMMONIUM

Both nitrogen and phosphorus are essential nutrients for plants and animals.

Nitrogen exists in water in the form of nitrate (NO_3). Excessive amounts of nitrate increase algae growth. Algae can rob the water of dissolved oxygen and eventually kill fish and other aquatic life. Sources of nitrate may include human and animal wastes, industrial pollutants and runoff from heavily fertilized croplands and lawns. Under certain conditions, high levels of nitrates (10 mg/L or more) in drinking water can be toxic to humans. High levels of nitrates in drinking water have been linked to serious illness and even death in infants [27]. The standard limits of nitrate in treated waste water is 30 mg/L.

In nature, phosphorus usually exists in the form of phosphate (PO_4). Since phosphorus is the nutrient in short supply in most fresh waters, even a modest increase in phosphorus can cause events including accelerated plant growth, algae blooms, low dissolved oxygen, and the death of certain fish, invertebrates, and other aquatic animals. The sources of phosphorus include: soil and rocks, wastewater treatment plants, runoff from fertilized lawns and cropland, failing septic systems, runoff from animal manure storage areas, disturbed land areas, drained wetlands, water treatment, and commercial cleaning preparations [27]. The standard levels for treated waste water and drinking water are approximately 20 mg/L and 4 mg/L, respectively.

Ammonium (NH_4) is one of the forms of nitrogen that exist in aquatic environments. Unlike other forms of nitrogen, which cause nutrient over-enrichment of a water body and indirectly affect aquatic life, ammonium causes direct toxic effects. It is produced for commercial fertilizers and other industrial applications. Natural sources of ammonium include: decomposition or breakdown of organic waste matter, gas exchange with the atmosphere, forest fires, animal and human waste, and nitrogen fixation processes. High levels of that in water makes it difficult for aquatic organisms to sufficiently excrete the toxicant, leading to toxic buildup in tissues and blood, and potentially death. Environmental factors, such as pH and temperature, can affect ammonia toxicity [27]. The typical standard level for ammonia in drinking water is 20 μg/L.

B. HEAVY METALS

The term heavy metal refers to any metallic chemical element that has a relatively high density and is toxic or poisonous at low concentrations in water. Examples of heavy metals include mercury (Hg), cadmium (Cd), arsenic (As), chromium (Cr), thallium (Tl), and lead (Pb). In this paper, we consider measuring Cr, Hg, and Pb.

Main sources of Cr contamination in drinking water include discharge from steel and pulp mills and erosion of natural deposits. Long-term exposure to high doses of Cr can cause Allergic dermatitis [27]. Typical standard levels for Cr in treated waste water and drinking water are 1 μg/L and 100 μg/L, respectively [27], [28].

Main sources of Hg contamination in drinking water include erosion of natural deposits, discharge from refineries and factories, and runoff from landfills and croplands. Long-term exposure to high doses of Hg can cause kidney damage [27]. Typical standard levels for Hg in treated waste water and drinking water are 5 μg/L and 2 μg/L, respectively.

Main sources of Pb contamination in drinking water are corrosion of household plumbing systems and erosion of natural deposits. Some potential health effects from long-term exposure to high doses of Pb include delays in physical or mental development of infants and children. Besides, children could show slight deficits in attention span and learning abilities. In adults, it causes kidney problems and high blood pressure [27]. Typical standard levels for Pb in treated waste water and drinking water are 50 μg/L and 15 μg/L, respectively.

C. PH

The pH of a body of water is a measurement of its acidity or alkalinity ranging from 0 to 14, with the lower values indicating acidic environments and the higher ones alkaline. A completely neutral pH has the value of 7. A one-point change in pH indicates a ten-fold change in the acidity or alkalinity of the body of water. According to New York State regulation 6 NYCRR Part 703.3 [29], pH shall not be less than 6 or greater than 9.5 for a Class D body of fresh surface water and shall not be less than 6.5 or greater than 8.5 in Classes AA, A, B, C, AA-Special, A-Special, or GA. Class D waters are suitable for fish, shellfish and wildlife survival, as well as for primary and secondary contact recreation. The other classes are better quality waters with AA-Special having the highest standards. Class GA represents potable groundwater. Drinking water supplies in New York State are set by the New York State Department of Health (NYSDOH). The acceptable pH range set by NYSDOH is 6.8 to 8.2 and is based upon the Federal Lead and Copper Rule [30].

D. DISSOLVED OXYGEN

A sufficient amount of dissolved oxygen (DO) in surface water is necessary to maintain a healthy ecosystem. Levels below 5 mg/L begin to put stress on aquatic life, and levels below 2 mg/L begin to result in fish kills. In New York State, the regulatory limits for DO vary depending upon the class of water [29]. For rivers and the hypolimnion of lakes, DO must not be under 6 mg/L. In trout spawning waters, the DO must not be under 7 mg/L. Class D surface water shall not be less than 3 mg/L. Measuring real-time DO in bodies of water may provide crucial data for public health impacts. Bacterial degradation of organic matter results in a drop of DO, indicating pollutants in that body of water [31]. A disruption to the food web is an outcome of aquatic dead zones resulting from oxygen deficient ecosystems [32].

E. CONDUCTIVITY

Water carries dissolved ions which, in turn, allows it to provide a flow of electricity [33]. Increased conductivity in fresh surface water indicates an increase in the amount of dissolved ions, while an increase in groundwater implies saltwater intrusion. Measuring the total dissolved solids (TDS) in water is often used alongside conductivity and provides a value for all ions and organic matter that are dissolved and smaller than 2 microns. The unit of TDS measure is mg/L. In New York State, TDS cannot exceed 500 mg/L in most waters, and cannot exceed 200 mg/L in waters that will be used for consumption.

III. IMPORTNACE OF REAL-TIME WATER QUALITY SENSING

Drinking water and wastewater systems most often have their own wet chemistry labs and the technologies are typical for that environment. For example, in New York City, the Department of Environmental Protection collects more than 1,300 water samples per month from up to 546 locations. These samples are collected by field personnel and analyzed for bacteria, chlorine levels, pH, inorganic and organic compounds, turbidity, odor, and many other water quality indicators in a drinking water quality laboratory. There are 965 sampling stations throughout the city with a construction cost of 11 million dollars [10]. Wastewater is measured at the influent, effluent, and treatment tanks in between. Wastewater treatment workers typically collect samples manually for a number of parameters at varying frequencies dependent upon the facility's discharge permit. Samples are sent to an onsite wet chemistry laboratory where temperature, pH, biological oxygen demand (BOD), and bacteria are quantified as well as any other parameters dictated by the permit. The technologies found in the laboratories are typical pieces of equipment, ranging from pH and dissolved oxygen meters to liquid chromatography systems. Results can be turned around from several hours to several days.

The above-mentioned common practices in water quality sensing indicate that the development of a water sensing technology that is fast, reliable, compact, and cost-effective is of high demand.

IV. DESIGN, FABRICATION, AND PARAMETRIC STUDY OF THE MICROWAVE SENOR ARRAY

In this section, we present the design of a microwave sensor array for water quality testing. The sensor array is composed

of five elements, each of which is designed based on a microstrip transmission line loaded with a complementary split ring resonator (CSRR) resonating at a different frequency within the range of 1 GHz to 10 GHz.

In general, a transmission line loaded with a resonant element (either coupled to it or in contact with it), such as split ring resonator (SRR) [34] or CSRR [35], exhibits a set of transmission zeros in the frequency response. These transmission zeros occur at those frequencies where the resonant element produces an open or a virtual ground to the line, and the injected power is completely reflected back at these frequencies (excluding the effects of losses). Typically, the frequency of interest for microwave circuit and sensor design is the first (fundamental) resonance frequency, where metamaterial-inspired resonators can be used in order to achieve compact dimensions. This frequency (and higher order harmonic frequencies) may be altered by the presence of substances/materials surrounding the resonant element. Therefore, the resonance frequency variation and the response level of the sensor at resonance can be used for sensing material characteristic changes. These sensors are useful in many applications where design simplicity and low cost are key aspects to consider.

Recently, resonant microwave sensors based on the planar microstrip line loaded with SRR [36] or CSRR [37]–[41] have been reported to determine the properties or other parameters of dielectric materials under test in microwave regime. The design of resonant sensors based on the planar technology has certainly many advantages such as its low cost, portability, non-invasiveness and flexibility of sample preparation. However, the configurations examined in the literature so far are mainly based on a single sensor element which provides material characterization only at one specific frequency.

It has been shown in [38] that CSRR sensor structure is more sensitive to changes in permittivity than SRR structure. Therefore, here, CSRR structure is selected for water sensing. In particular, an array of five CSRRs are used for sensing major parameters and pollutants in water as shown in FIGURE 1. The CSRRs are etched out of a ground plane on the surface of a substrate with a microstrip line on the opposite surface of the substrate. This configuration for sensor array can be fabricated in a cost-effective way through printed circuit board (PCB) technology.

The CSRR structure has a planar shape with a center island connected to the surrounding ground planes by narrow lines. When there is a voltage difference between the center island and the surrounding ground plane, the current experiences a capacitance between the island and the ground plane and an inductance at the narrow lines that connects the two. Therefore, depending on the capacitance and the inductance, resonant behavior is observed. Typically, larger CSRR dimensions are associated with lower resonant frequencies, as larger dimensions entail higher inductance and higher capacitance. When exciting the microstrip from one end, the electromagnetic fields travel through the microstrip transmission line from one end to another. The split rings on
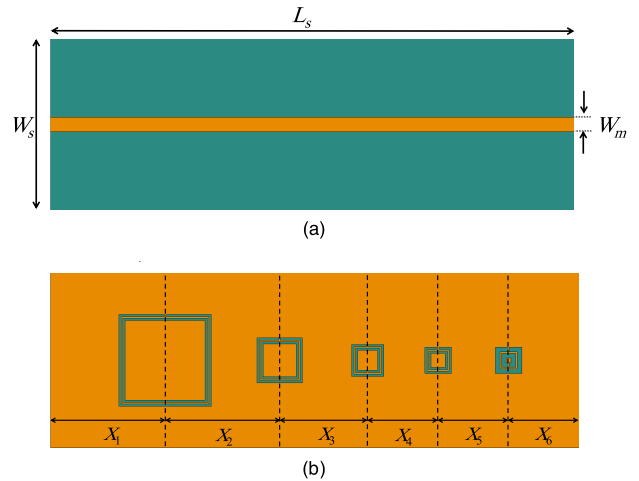

FIGURE 1. Microwave sensor array (a) front surface and (b) back surface with Sensor 1 to Sensor 5 shown from left to right, respectively, each of which corresponds to an increasing resonance frequency.

the ground surface can affect the current in the microstrip line leading to resonances at certain frequencies.

The sensor array in FIGURE 1 allows for measuring the change in the dielectric properties of water over a wide frequency range from 1 GHz to 10 GHz. Specifically, the sensor array presented here contains elements resonating at five frequencies around 1 GHz, 3 GHz, 5 GHz, 7 GHz and 9 GHz. The change in the dielectric properties can be then monitored through measuring both resonance frequency shifts and amplitude changes of the responses at resonance frequencies.

The sensor design is implemented and evaluated using Altair FEKO simulation software [42] which is based on method of moments (MoM). The substrate is chosen to be Rogers RO4350 with dielectric properties of $\varepsilon_r = 3.66$ and $\tan \delta = 0.0031$. The width W_s and length L_s of substrate are 20 mm and 56 mm, respectively. The thickness of the substrate is 0.75 mm. A microstrip line with characteristic impedance of 50 Ω (width of strip line is $W_m = 1.68$ mm) is placed at the center of the front surface of the substrate. On the back side of the substrate, there is a ground plane with five CSRRs etched out of that. The CSRRs, as shown in FIGURE 1(b), are named Sensor 1 to Sensor 5 from left to right, each of which corresponds to an increasing resonance frequency.

FIGURE 2 shows the design parameters for each sensor including the length of the outer ring L, width of the rings W, the track between adjacent rings b, and the width of narrow lines a. As a rule of thumb, a larger value of L corresponds to a lower resonance frequency and as W increases, the resonance frequency decreases.

In this paper, considering the fabrication limits, we restrict the minimum width of tracks and gaps to be 0.16 mm or larger. The sensors are then placed on the same substrate as shown in FIGURE 1(b) to construct the sensor array. Further fine-tuning is conducted for the complete model. The final design parameters and center-to-center distances for the sensor array are shown in Table 1 and Table 2, respectively.
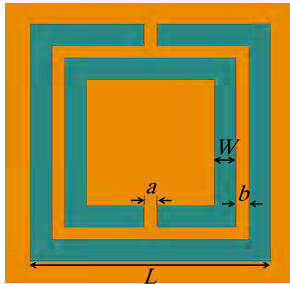
FIGURE 2. Parametric model of each CSRR.

TABLE 1. Dimensions of the designed CSRRs.

	f_r (GHz)	W (mm)	L (mm)	a (mm)	b (mm)
Sensor 1	1.36	0.27	10.5	0.16	0.16
Sensor 2	3.09	0.27	5.15	0.16	0.16
Sensor 3	5	0.27	3.65	0.16	0.16
Sensor 4	6.82	0.27	3	0.16	0.16
Sensor 5	8.91	0.54	3	0.16	0.16

TABLE 2. Distance between CSRRs as shown in Figure 1(b).

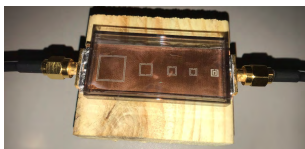| X_1 (mm)	X_2 (mm)	X_3 (mm)	X_4 (mm)	X_5 (mm)	X_6 (mm)
11	13	10	8	8	6

FIGURE 3. Fabricated sensor array.

FIGURE 3 shows the fabricated sensor array. In order to test water samples, a plexiglass container with thickness of bottom surface $t = 1.6$ mm is installed on the back surface of the device including all the CSRRs. Then, SMA connectors are soldered on both ends of the microstrip transmission line. Finally, the whole device is installed on a piece of wood stand to ensure a mechanically stable platform for conducting the measurements.

To monitor the response of the sensor array to water solutions, the variation of transmission S-parameter $|S_{21}|$ versus frequency is measured using a vector network analyzer (E5063A ENA from Keysight Technologies) as shown in FIGURE 4. FIGURE 5 shows the variation of the simulated $|S_{21}|$, compared with the one measured for the fabricated sensor array with the empty container as well as the case in which the container is filled with distilled water. It is observed that reasonable match is observed between the simulated and measured results (for empty container). The mis-matches can be due to the use of container in the measurement (it was absent in the simulation model), fabrication tolerances, and soldering.

It is worth noting that since the sensitivity and selectivity of CSRR-based sensors rely on the high Q of the elements, placement of the CSRRs next to a medium with substantial loss can significantly lower the Q of the elements, which, in turn, results in significant deterioration of the sensing accuracy. This issue has been also pointed out in [37], [38]. In particular, it has been shown in [37] that increasing the
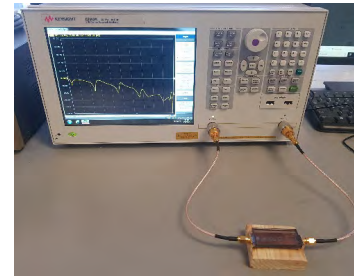

FIGURE 4. Measurement of $|S_{21}|$ for the sensor array with a vector network analyzer (E5063A ENA from Keysight technologies).
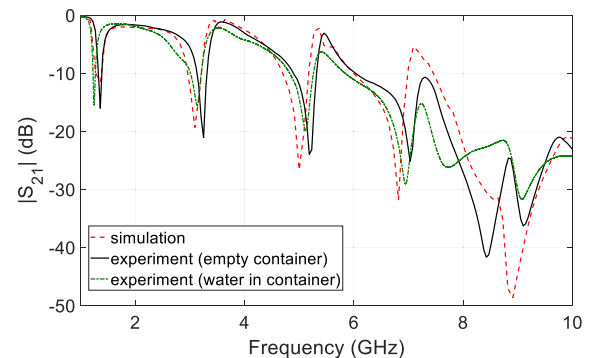

FIGURE 5. Simulated and measured $|S_{21}|$ for the sensor array.

thickness of a Teflon film between the CSRR element and a metal (aluminum) under test, improves the sensitivity of the sensor. Here, since CSRRs are used for sensing water which is a lossy material (specially, if it contains heavy metal contaminants), we use a container with a certain thickness of bottom surface t. Choosing a container with proper value of t is crucial. An excessively thin container (if t is too small) leads to lower Q of the resonators and lower sensitivity. On the other hand, an excessively thick container (if t is too large) may also decrease the sensitivity of the responses to the water samples due to a larger distance between the water samples and regions of field concentrations on CSRRs. Including this effect in the FEKO simulation model to optimize t is not straight-forward. This is due to the fact that the commercial dielectric probe kit utilized in this project does not provide reliable measured property values for high conductivity solutions, i.e., water solutions with heavy metal inclusions, as discussed later. As mentioned earlier, in this work, we used a plexiglass container with $t = 1.6$ mm.

To further study the effect of thickness of the container t (distance between the sample and CSRRs) and the volume of the container, we conduct measurements with four containers as shown in FIGURE 6. The container in FIGURE 6(a) is the original one used in water sample measurements with $t = 1.6$ mm. The container in FIGIRE 6(b) has lower thickness as $t = 0.8$ mm. The containers in FIGURES 6(c) and 6(d) have similar thickness t as the original container but have larger volumes. Tables 3 shows the dimensions of these four containers. FIGURE 7 shows the measured responses when these four containers are filled with distilled water and using another fabricated sensor array. It is observed that the quality
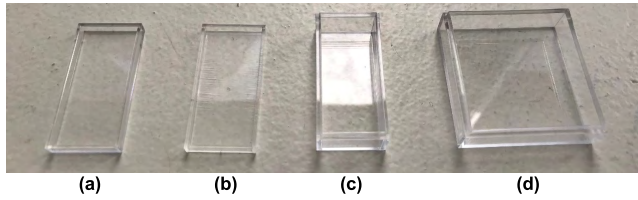
FIGURE 6. The containers used to study the effect of distance between water sample and CSRRs and the container volume, (a) original container used in the water sample measurements, (b) thinner container, (c) larger container NO. 1, (d) larger container No. 2. Dimensions of these containers are shown in Table 3.
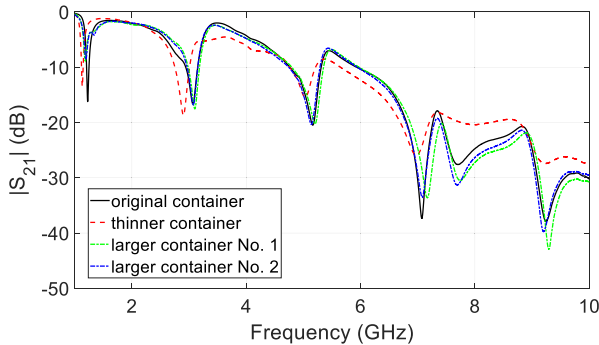

FIGURE 7. Measured $|S_{21}|$ for another fabricated sensor array when using the four containers shown in FIGURE 6 with dimensions shown in Table 3 and filled with distilled water.

TABLE 3. Dimensions of containers used to study the effect of distance between water sample and CSRRs and container volume.

Container	Dimensions	Thickness (t)
Original container	25mm×50mm×5.7mm	1.6mm
Thinner container	25mm×50mm ×4.9mm	0.8mm
Larger container No. 1	25mm×50mm ×15.8mm	1.6mm
Larger container No. 2	50mm×50mm×15.8mm	1.6mm

factors for the resonances deteriorate for the thinner container compared to the original one as expected and discussed in the previous paragraph. The responses for larger containers do not show deterioration of quality factors except at the lowest resonant frequency. This could be due to the fact that at larger wavelengths, the field is affected (attenuated with the lossy water sample) over a larger distance from the CSRR structure.

Next, to study the effect of distances between CSRRs and substrate edge effects, we conduct a simulation study. In a first model the distances X_1 to X_6 reported in Table 2 are doubled. In a second model, the width of the substrate W_s is doubled as well in addition to doubling distances X_1 to X_6. FIGURE 8 compares the responses of these models with the original design. It is observed that, in particular, doubling the distances X_1 to X_6 has some effects on the quality factors of the CSRR resonators. This study also helps to understand the reason for the decrease in the $|S_{21}|$ level at higher frequencies. It shows that this effect is not due to the mutual effect between the CSRR structures or the substrate edge effects. Instead, we conclude that this effect is mainly due to the loss of power in the form of radiation from CSRR structures. This conclusion was further validated via simulation of a single CSRR structure over a large substrate.
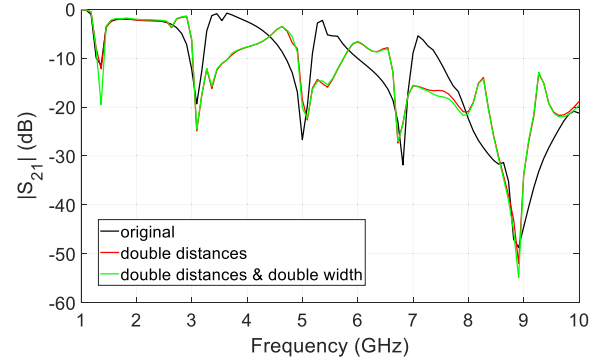

FIGURE 8. Simulated $|S_{21}|$ for the original design, a model with doubling the distances X_1 to X_6 in Table 2 (referred to as double distances in the plot), and a model with doubling the distances X_1 to X_6 in Table 2 and doubling the width of the substrate W_s (referred to as double distances & double width in the plot).
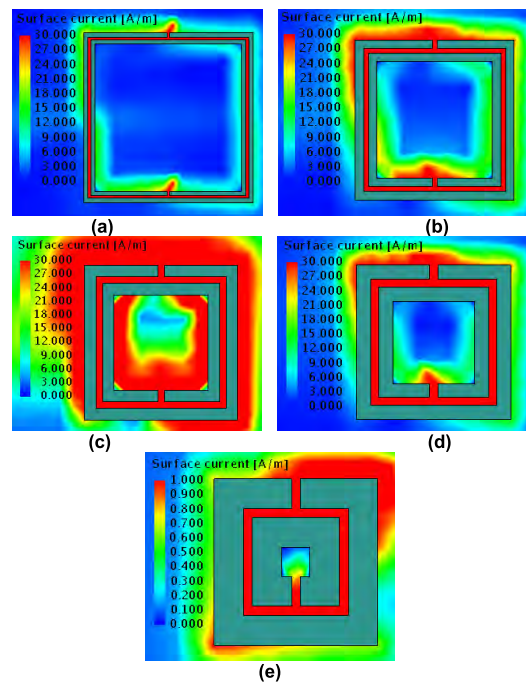

FIGURE 9. Current distributions of each sensor at its resonant frequency: (a) Sensor 1 at 1.36 GHz, (b) Sensor 2 at 3.09 GHz, (c) Sensor 3 at 5 GHz, (d) Sensor 4 at 6.82 GHz, and (e) Sensor 5 at 8.91 GHz.

In the simulation model, we also observe the current distribution around each sensor as shown in FIGURE 9. Investigation of the current distribution on a CSRR at the resonance frequency shows the critical locations at which the electromagnetic energy is concentrated. It is observed that the current distributions are maximum at the region around the CSRRs which make these regions sensitive to variations of the fields due to the changes in the material properties.

V. EVALUATIONS AND RESULTS

In this section, we first introduce the water solutions employed in this study. Next, the dielectric properties of the samples are measured with a commercial dielectric probe kit and then the responses to these samples are presented for the sensor array.

Sample	Concentration in water or parameter values
Nitrate (NO_3)	100 μg/mL
Phosphate (PO_4)	100 μg/mL
Ammonium (NH_4)	100 μg/mL
Lead (Pb)	10 μg/mL
Mercury (Hg)	1000 μg/mL
Chromium^{+6}(Cr^{+6})	10 μg/mL
PH levels	4, 7, and 10
NaCl	6440 and 40000 μg/mL
Dissolved Oxygen (DO)	0 mg/L
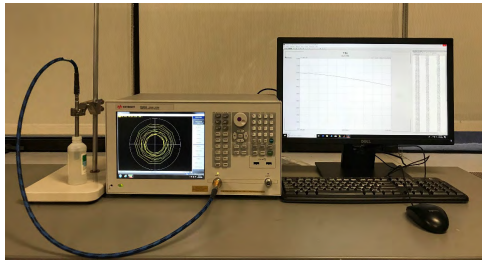
FIGURE 10. Measurement of dielectric properties of the water solutions with a dielectric probe kit and vector network analyzer.

FIGURE 11. Variation of permittivity versus frequency measured with dielectric probe kit for distilled water compared with water solutions with ammonium, nitrate, and phosphate: (a) real part and (b) imaginary part.
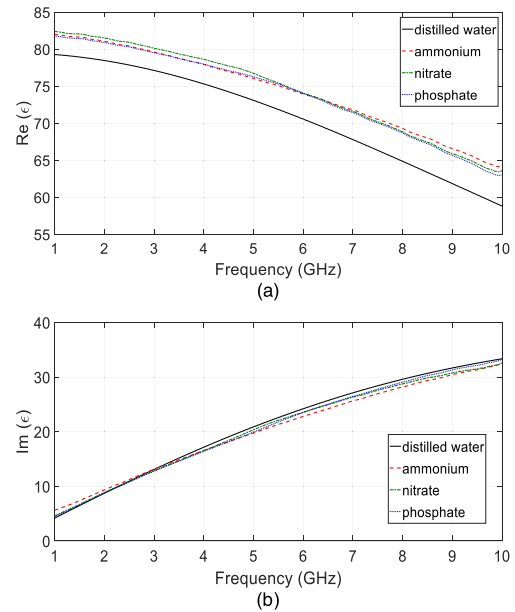
A. WATER SAMPLES USED IN EVALUATING THE PERFORMANCE OF THE MICROWAVE SENSOR

In this section, we present the water samples used to evaluate the performance of the microwave sensor array. We used commercial solutions of different contaminants. Table 4 shows the commercial samples used in the study and their corresponding concentration levels or parameter values. In order to provide various conductivities, sodium chloride (NaCl) has been dissolved in water with concentration levels indicated in Table 4. Approximately, each mg/L of NaCl produces conductivity of 2 μS/cm. Besides, our DO sample has concentration of 0 mg/L. It is composed of 5% of Sodium Sulfite (Na_2SO_3), less than 0.001% of Cobalt Chloride Hexahydrate ($CoCl_2.6H_2O$), and more than 94% of deionized water (H_2O). This indicates that this solution has large conductivity (highly lossy material).

In the following sections, we present the measured dielectric properties as well as the measured responses of the sensor array to these water samples. As discussed in section V.C, some of the samples are diluted with distilled water to study the sensitivity of the responses.

B. MEASUREMENT OF DIELECTRIC PROPERIES WITH A DIELECTRIC PROBE KIT

In order to better understand the responses of the sensor array, first, the dielectric properties of the distilled water and the water solutions are measured with a Keysight Dielectric probe kit (performance probe N1501A) together with the relevant measurement Software N1500A and a vector network analyzer (E5063A from Keysight). Here, the real and imaginary parts of permittivity are denoted by $Re(\varepsilon) = \varepsilon_r$ and $Im(\varepsilon) = \varepsilon_i$, respectively. FIGURE 10 shows the dielectric measurement setup. The measurements are conducted after calibrating the dielectric probe with measurements taken using distilled water, open, and short components. Then, the real and imaginary parts of the permittivity are measured within the frequency range of 1 GHz to 10 GHz. FIGURE 11 to FIGURE 13 show the results. A table that summarizes the permittivity of samples under test is presented in the Appendix for easier reference. Please note that according to the manufacturer of the dielectric probe kit (KeySight Technologies), the dielectric property measurements may not be reliable for samples with high conductivity in microwave regime. This was also observed in our measurements (measurements were not repeatable and reasonable for such solutions). Thus, here, we exclude dielectric property measurement results for water solutions with heavy metals and DO which have very high conductivities within microwave frequency range.

FIGURE 11 shows that the water solutions with ammonium, nitrate, and phosphate show a noticeable change in ε_r compared to distilled water. However, their ε_r values do not differ much (from each other) in the measured frequency range. Besides, it is observed that ε_i does not change much compared to distilled water for these solutions. The property measurements for these three solutions indicate that it is difficult to distinguish these water solutions from each other. However, it is still possible to detect them and distinguish this category of samples from distilled water.

FIGURE 12 shows the variation of ε_r and ε_i for water solutions with pH levels of 4, 7, and 10. It is observed that ε_r values differ from distilled water at higher frequencies (around 6 GHz) while ε_i values have larger differences with distilled water at lower frequencies (around 4 GHz). Also, different levels of pH are better discernable from ε_i values at lower frequencies rather than ε_r values at higher frequencies.

FIGURE 12. Variation of permittivity versus frequency measured with dielectric probe kit for distilled water compared with water solutions with pH levels of 4, 7, and 10: (a) real part and (b) imaginary part.
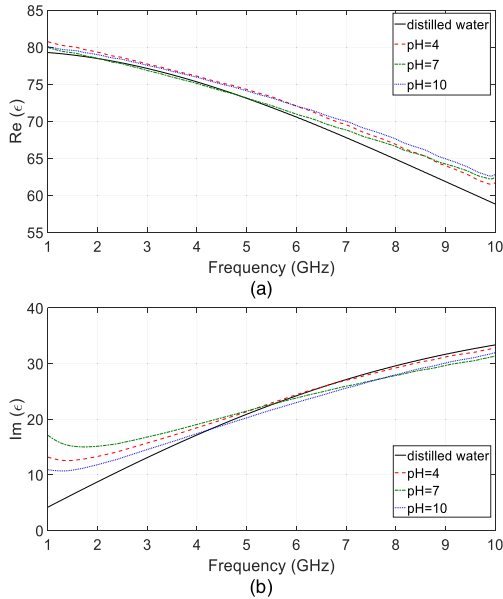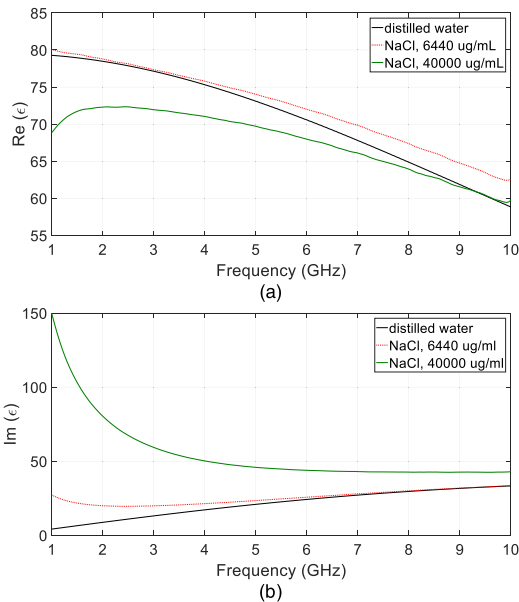

FIGURE 13. Variation of permittivity versus frequency measured with dielectric probe kit for distilled water compared with water solutions with NaCl with concentrations of 6440 and 40000 ug/mL: (a) real part and (b) imaginary part.

FIGURE 13 shows the variations of ε_r and ε_i for water solutions with NaCl concentrations of 6440 and 40000 μg/mL. As described in section V.A, higher concentrations of NaCl corresponds to higher water conductivities. It is observed that with higher levels of conductivity, the values of ε_r and ε_i differ more from those of distilled water.

C. MEASUREMENTS AND ANALYSIS OF RESPONSES FOR MICROWAVE SENSOR ARRAY

In this section, we present the results of measuring responses of the microwave sensor array when the sensor is exposed
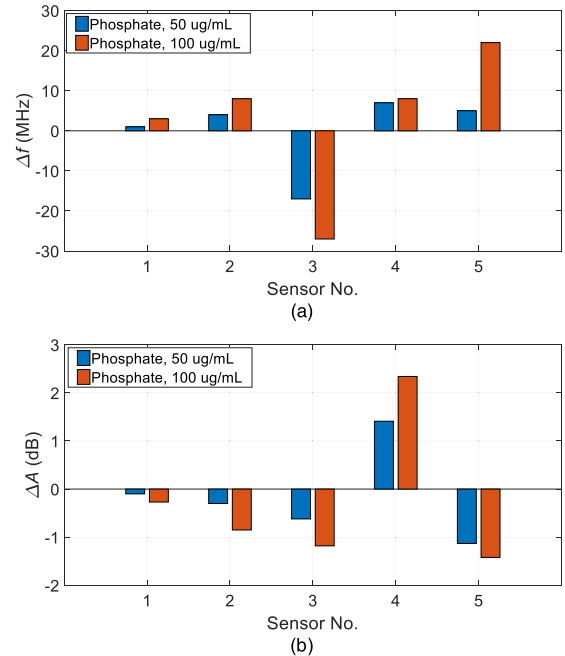

FIGURE 14. Response changes due to water solutions with two concentrations of phosphate with respect to distilled water: (a) Δf and (b) ΔA.

to water solutions presented in section V.A. The response of the sensor ($|S_{21}|$) is measured with a Keysight E5063A vector network analyzer. As discussed earlier, to measure the samples, a plexiglass container with bottom thickness of 1.6 mm is placed on the back surface of the sensor to cover the CSRRs on the ground sheet.

FIGURE 14 to FIGURE 20 show the differences in the resonance frequencies (Δf) and the differences in their corresponding values of $|S_{21}|$(ΔA) at resonance frequencies with respect to distilled water. In order to observe the sensitivity of the sensors to various concentrations of contaminants, we dilute some of the samples discussed in section V.A to lower concentrations using distilled water. The concentration of the diluted samples will be discussed along with the obtained responses in the following.

The complex dielectric values for ammonium, nitrate, and phosphate are very close as shown in FIGURE 11. Thus, here, we present the sensor array response only for phosphate since others provide similar results. FIGURE 14 shows the variation of Δf and ΔA for two concentration levels of phosphate: 50 ug/mL and 100 ug/mL. It is observed that the values of Δf and ΔA increase with the increase of the concentration level for all the sensor elements. Sensor 3 shows the largest Δf values while Sensor 4 shows the largest ΔA values. In general, all sensors show measurable Δf values (Δf larger than 1 MHz). For ΔA values, mainly, Sensors 4 and 5 show more robust responses with ΔA larger than 1 dB.

FIGURE 15 shows the variation of Δf and ΔA for two concentration levels of Cr: 5 ug/mL and 10 ug/mL. It is observed that the values of Δf and ΔA increase with the increase of the concentration level for all the sensor elements. Sensor 5 shows the largest Δf values while Sensor 4 shows

FIGURE 15. Response changes due to water solutions with two concentrations of Cr with respect to distilled water: (a) Δ*f* and (b) Δ*A*.

FIGURE 16. Response changes due to water solutions with two concentrations of Hg with respect to distilled water: (a) Δ*f* and (b) Δ*A*.
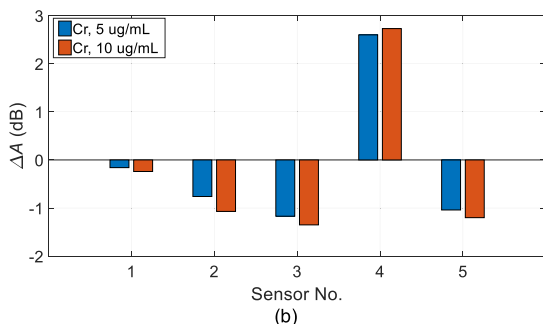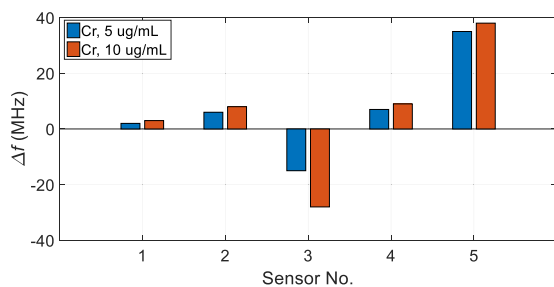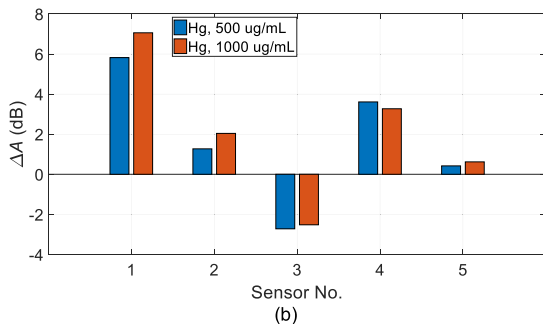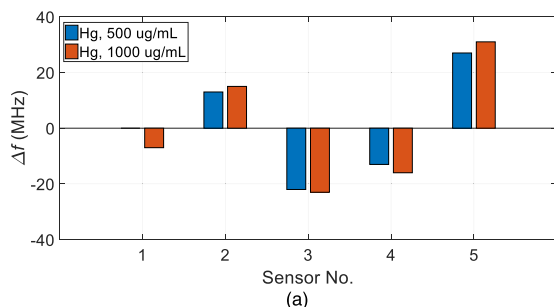

FIGURE 17. Response changes due to water solutions with two concentrations of Pb with respect to distilled water: (a) Δ*f* and (b) Δ*A*.

the largest Δ*A* values. In general, all sensors show measurable Δ*f* values (Δ*f* larger than 1 MHz). For Δ*A* values, Sensors 3 to 5 show more robust responses with Δ*A* larger than 1 dB.

FIGURE 16 shows the variation of Δ*f* and Δ*A* for two concentration levels of Hg: 500 ug/mL and 1000 ug/mL. It is observed that, in general, the values of Δ*f* and Δ*A* increase with the increase of the concentration level for all the sensor elements. However, few non-linear responses are observed. The values of Δ*A* for Sensors 3 and 4 actually decrease with the increase of the concentration level. Sensor 5 shows the
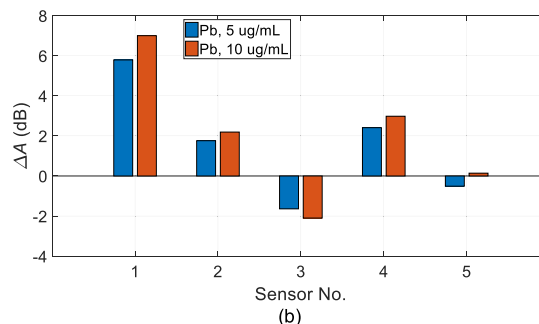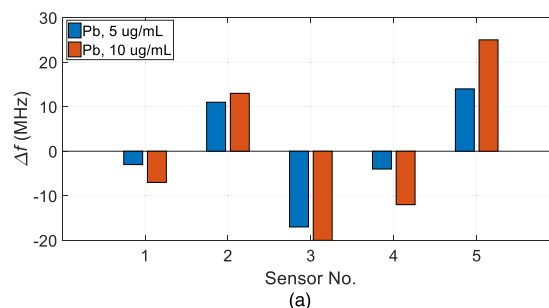
largest Δ*f* values while Sensor 1 shows the largest Δ*A* values. In general, all sensors show measurable Δ*f* values (Δ*f* larger than 1 MHz) except for the Sensor 1 response for the lowest concentration level which is below 1 MHz. For Δ*A* values, Sensors 1 to 4 show robust responses with Δ*A* values larger than 1 dB.

FIGURE 17 shows the variation of Δ*f* and Δ*A* for two concentration levels of Pb: 5 ug/mL and 10 ug/mL. It is observed that, in general, the values of Δ*f* and Δ*A* increase with the increase of the concentration level for all the sensor elements. However, one non-linear response is observed. The value of Δ*A* for Sensor 5 actually decreases with the increase of the concentration level. Sensors 3 and 5 show the largest Δ*f* values while Sensor 1 shows the largest Δ*A* values. All sensors show measurable Δ*f* values (Δ*f* larger than 1 MHz). For Δ*A* values, Sensors 1 to 4 show robust responses with Δ*A* larger than 1 dB.

FIGURE 18 shows the variations of Δ*f* and Δ*A* for three pH levels of the water: 4, 7, and 10. It is observed that almost all sensors show measurable responses with Δ*f* values larger than 1 MHz. While Sensor 1 and Sensor 3 show decrease of Δ*f* with the increase of pH level, Sensors 4 and 5 show increase of Δ*f* with respect to the increase in pH level. In general, the largest Δ*f* responses are observed for Sensor 5 which is consistent with ε*r* measurement in FIGURE 12(b), showing the largest variation of ε*r* for pH solutions at higher frequencies. For Δ*A*, also almost all sensors show measurable values with Δ*A* larger than 1 dB. Sensors 3 and 4 show the largest Δ*A* values.

FIGURE 19 shows the variation of Δ*f* and Δ*A* for two concentration levels of NaCl: 6440 ug/mL and 40000 ug/mL. It is observed that, in general, the values of Δ*f* and Δ*A* increase with the increase of the concentration level for all the sensor
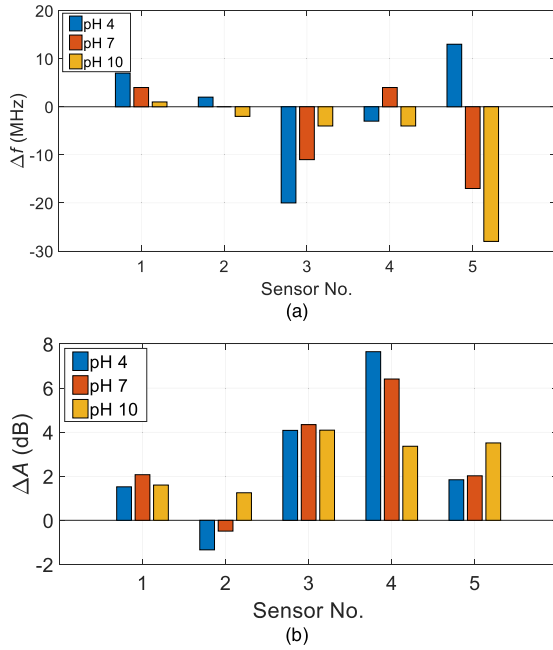
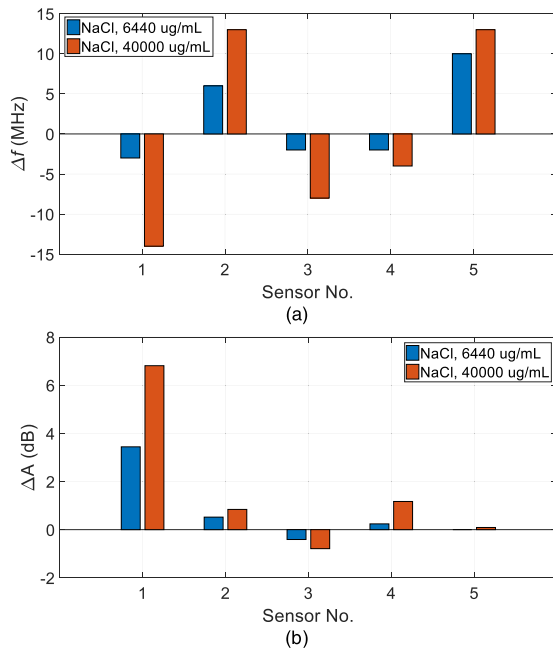**FIGURE 18.** Response changes due to water solutions with three pH levels with respect to distilled water: (a) Δf and (b) ΔA.

FIGURE 19. Response changes due to water solutions with two concentrations of NaCl with respect to distilled water: (a) Δf and (b) ΔA.

FIGURE 20. Response changes due to water solutions with DO of 0 mg/L with respect to distilled water: (a) Δf and (b) ΔA.

TABLE 5. Real part of permittivity versus frequency measured with dielectric probe kit for distilled water compared with water solutions with ammonium, nitrate, and phosphate.

Frequency	Water	Ammonium	Nitrate	Phosphate
1 GHz	79.3	82.0	82.4	81.8
2 GHz	78.6	81.1	81.6	81.0
3 GHz	77.4	79.6	80.1	79.5
4 GHz	75.9	77.9	78.6	78.0
5 GHz	74.0	76.1	76.8	76.3
6 GHz	71.9	73.9	74.0	73.9
7 GHz	69.5	71.9	71.8	71.5
8 GHz	66.9	69.4	68.9	68.7
9 GHz	64.3	66.5	65.8	65.6
10 GHz	61.4	64.3	63.6	63.1

TABLE 6. Imaginary part of permittivity versus frequency measured with dielectric probe kit for distilled water compared with water solutions with ammonium, nitrate, and phosphate.

Frequency	Water	Ammonium	Nitrate	Phosphate
1 GHz	4.2	5.6	4.6	4.5
2 GHz	8.3	9.3	8.9	8.8
3 GHz	12.2	13.1	12.9	12.8
4 GHz	16.0	16.6	16.5	16.4
5 GHz	19.5	19.8	20.4	20.0
6 GHz	22.6	22.8	23.5	23.6
7 GHz	25.4	25.6	26.3	26.4
8 GHz	27.9	28.3	28.9	29.1
9 GHz	30.0	30.3	30.6	31.2
10 GHz	31.9	32.6	32.6	33.3

elements. The largest value of Δf is observed for Sensor 1 and for higher NaCl concentration. This is consistent with the ε_r measurement results in FIGURE 13(a). Besides, the largest values of ΔA are observed for Sensor 1 which is also consistent with ε_i measurement results in FIGURE 13(b). All sensors show measurable Δf values (Δf larger than 1 MHz). For ΔA values, Sensor 1 shows reliable measurement values while other sensors' responses are around or lower than 1 dB.
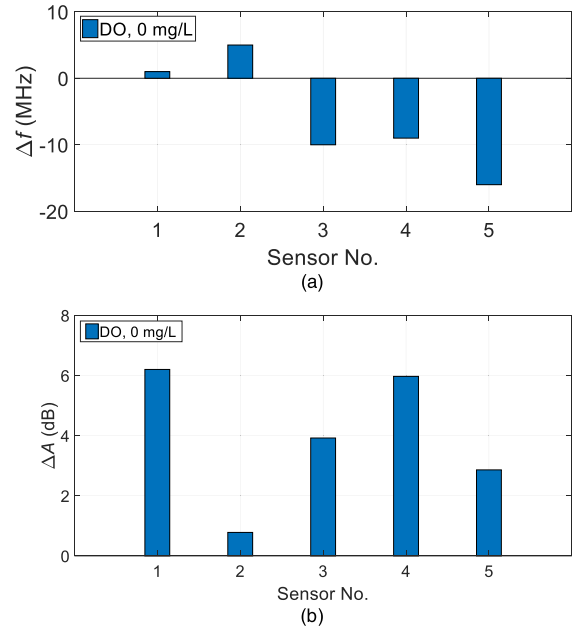
FIGURE 20 shows the variation of Δf and ΔA for 0 mg/L of DO. It is observed that, in general, all the sensors show measurable values for both Δf and ΔA except Sensor 2 that shows very small ΔA value, i.e., smaller than 1 dB. Sensor 5 shows the largest Δf value while Sensors 1 and 4 show the largest ΔA values.

TABLE 7. Real part of permittivity versus frequency measured with dielectric probe kit for distilled water compared with water solutions with PH Level of 4, 7, and 10.

Frequency	Water	pH 4	pH 7	pH 10
1 GHz	79.3	80.7	80.0	80.1
2 GHz	78.6	79.4	78.6	79.1
3 GHz	77.4	77.6	76.7	77.4
4 GHz	75.9	76.1	75.1	76.1
5 GHz	74.0	74.4	73.2	74.2
6 GHz	71.9	71.9	70.8	71.9
7 GHz	69.5	69.7	69.0	70.2
8 GHz	66.9	67.0	66.7	67.7
9 GHz	64.3	63.9	64.0	64.7
10 GHz	61.4	61.7	62.5	62.9

TABLE 8. Imaginary part of permittivity versus frequency measured with dielectric probe kit for distilled water compared with water solutions with PH levels of 4, 7, and 10.

Frequency	Water	pH 4	pH 7	pH 10
1 GHz	4.2	13.2	17.1	10.9
2 GHz	8.3	13.3	15.1	11.8
3 GHz	12.2	15.8	16.8	14.6
4 GHz	16.0	18.4	19.0	17.4
5 GHz	19.5	21.5	21.6	20.3
6 GHz	22.6	24.5	23.9	23.0
7 GHz	25.4	26.9	25.8	25.5
8 GHz	27.9	29.4	28.0	28.2
9 GHz	30.0	31.1	29.5	29.9
10 GHz	31.9	32.8	31.3	32.0

TABLE 9. Real part of permittivity versus frequency measured with dielectric probe kit for distilled water compared with water solutions with NaCl.

Frequency	Water	6440 (mg/L)	40000 (mg/L)
1 GHz	79.3	81.1	68.8
2 GHz	78.6	80.2	72.3
3 GHz	77.4	78.7	71.8
4 GHz	75.9	77.3	71.1
5 GHz	74.0	75.5	69.8
6 GHz	71.9	72.7	67.7
7 GHz	69.5	70.5	66.3
8 GHz	66.9	67.7	64.0
9 GHz	64.3	64.6	61.4
10 GHz	61.4	62.4	59.7

TABLE 10. Imaginary part of permittivity versus frequency measured with dielectric probe kit for distilled water compared with water solutions with NaCl.

Frequency	Water	6440 (mg/L)	40000 (mg/L)
1 GHz	4.2	27.2	149.9
2 GHz	8.3	20.0	80.5
3 GHz	12.2	19.8	59.3
4 GHz	16.0	21.4	50.1
5 GHz	19.5	23.6	46.0
6 GHz	22.6	25.6	43.9
7 GHz	25.4	28.0	42.9
8 GHz	27.9	30.1	42.9
9 GHz	30.0	31.7	42.4
10 GHz	31.9	33.6	42.9

In general, it is observed that the changes in the responses due to the tested water solutions are measurable for many of the sensors. To justify that, here, we refer to sample works in the literature, in which, VNA has been used to measure response changes of the resonance-based microwave sensors. For instance, response changes as low as 0.1 dB in $|S_{21}|$ and 0.1 MHz in the resonance frequency have been reported in [43]. Also, measurable resonance frequency change of 10 KHz has been reported in [44]. Here, in general, the reported results for Δf and ΔA are much larger ensuring the accurate measurements with VNA. Besides the repeatability of the measurements have been validated via performing the testes multiple times at the room temperature.

VI. CONCLUSIONS AND DISCUSSIONS

In this paper, we present a microwave sensor array based on five compact CSRRs for water quality testing. The sensor elements operate at different frequencies covering a wide frequency band from 1 GHz to 10 GHz. This is, to our best knowledge, the first time that a microwave sensor array is studied for water quality testing. Operating over a wideband frequency range allows for acquisition of larger amounts of data that would, in turn, increase the detection and evaluation accuracy. Since the sensor array can be fabricated using conventional PCB technology, it can be mass-produced and distributed over vast bodies of water such as lakes, water reservoirs, etc.

For a compact and cost-effective sensing device, VNA needs to be replaced with an inexpensive data acquisition system. For this purpose, the sensor array structure has the advantage of easy integration with RF and microwave circuits. Sample readout circuits that can replace VNA have been presented based on the direct detection (homodyne) [45] and heterodyne detection schemes [46]. Alternatively, the sensor array can be adapted to wireless data acquisition techniques, similar to RFID sensor technology (e.g., see [47]). This would be an important step toward fast data acquisition for a large number of sensors covering a wide area. Such configuration addresses the scalability issue of conventional lab-based water testing approaches to quickly test vast bodies of water. In particular, techniques similar to the UWB chipless RFID proposed in [48] are attractive. However, one drawback of these systems is that the signal to noise ratio (SNR) will be lower than a VNA measurement system. As explained in detail in [48], the useful signal returned back by the sensing system and measured by the reader antenna is affected by many factors which, in turn, reduce the SNR in a wireless data acquisition technique as compared to VNA measurements leading to lower dynamic range of the sensing system.

The sensor array was tested with water solutions with pollutants such as nitrate, phosphate, ammonium, and heavy metals (Hg, Pb, Cr). It was also tested with water samples with different levels of pH, NaCl (conductivity), and DO. The preliminary results show that using an array with elements operating at different frequencies is very beneficial. This is due to the fact that while some sensors may not respond to a particular contaminant, others can provide noticeable and readable responses. Besides, it is observed that frequency shift and change in the level of the response at resonance fre-

quency are both important parameters to consider for detection and evaluation of the water contaminants and parameters.

Future work includes using proper machine learning and pattern recognition algorithms to autonomously detect the contaminant in water and evaluate its concentration. We believe that using such post-processing tools allows for more accurate detection and evaluation of water samplers since a decision is made based on a pattern (vector of numbers) produced by the senor array. This is in contrast to the single sensor systems, in which, the decision is made only based on single response values.

Furthermore, the effects of ambient parameters, most importantly temperature, have to be studied in detail. Reducing such effects is necessary to have reliable water testing outcome. To reduce the effect of temperature, two approaches can be implemented, in practice. First, the temperature of the sample can be read and entered as a parameter in the post-processing algorithms. Such algorithms should have been trained with *a priori* data to calibrate out the temperature effect. Alternatively, calibration with respect to the temperature can be implemented by using differential responses for two sensors kept at the same temperature: one sensor exposed to distilled water and the other one exposed to the tested sample. The post-processing algorithms should be trained for such differential responses then.

APPENDIX

In this Appendix, we present the dielectric properties of the solutions measured in section V.B in table format (Tables 5 to 10). For brevity, The ε_r and ε_i values are down-sampled to present the values at frequencies 1 GHz to 10 GHz with steps of 1 GHz.

## REFERENCES

[1] *Water Security—The Water-Food-Energy-Climate Nexus*, Island Press, World Economic Forum, Washington, DC, USA, 2011.

[2] *The Water-Energy-Food Nexus: A New Approach in Support of Food Security and Sustainable Agriculture*, Food Agricult. Org. United Nations, FAO, Rome, Italy, 2014.

[3] J. C. Buzby, H. F. Wells, and J. Hyman, "The estimated amount, value, and calories of postharvest food losses at the retail and consumer levels in the United States," Dept. Agricult., U.S. Econ. Res. Service, Washington, DC, USA, Tech. Rep. EIB-121, Feb. 2014.

[4] M. Jalava, M. Kummu, M. Porkka, S. Siebert, and O. Varis, "Diet change—A solution to reduce water use?" *Environ. Res. Lett.*, vol. 9, no. 7, 2014, Art. no. 074016.

[5] M. Ivanova, "Global environmental outlook 5, united nations environment programme: Chapter 17, global responses," Conflict Resolution, Hum. Secur., Global Governance, Univ. Massachusetts Boston, Boston, MA, USA, Tech. Rep. 1-1-2012, 2012.

[6] J. Holden, P. M. Haygarth, J. MacDonald, A. Jenkins, A. Sapiets, H. G. Orr, and N. Dunn, "Agriculture's impacts on water quality," Global Food Secur., Swindon, U.K., Tech. Rep. 1, 2015.

[7] M. Wines, "Toxic algae outbreak overwhelms a polluted Ohio river," New York Times, Sep. 30, 2015. [Online]. Available: http://www.nytimes.com/2015/10/01/us/toxic-algae-outbreak-overwhelms-a-polluted-ohio-river.html?_r=0

[8] J. G. Hering, T. D. Waite, R. G. Luthy, J. E. Drewes, and D. L. Sedlak, "A changing framework for urban water systems," *Environ. Sci. Technol.*, vol. 47, no. 19, pp. 10721–10726, 2013.

[9] P. G. Whitehead, R. L. Wilby, R. W. Battarbee, M. Kernan, and A. J. Wade, "A review of the potential impacts of climate change on surface water quality," *Hydrol. Sci. J.*, vol. 54, no. 1, pp. 101–123, 2009.

[10] *NYC Department of Environmental Protection, Drinking Water Sampling Stations*. Accessed: May 30, 2019. [Online]. Available: https://www1.nyc.gov/site/dep/water/water-monitoring.page

[11] J. Goldman, N. Ramanathan, R. Ambrose, D. A. Caron, D. Estrin, J. C. Fisher, R. Gilbert, M. H. Hansen, T. C. Harmon, J. Jay, W. J. Kaiser, G. S. Sukhatme, and Y. Tai, "Distributed sensing systems for water quality assessment and management," Woodrow Wilson Int. Center Scholars, Washington, DC, USA, White Paper, 2007.

[12] A. Whittle, M. Allen, A. Preis, and M. Iqbal, "Sensor networks for monitoring and control of water distribution systems," in *Proc. 6th Int. Conf. Struct. Health Monit. Intell. Infrastruct. (SHMII)*, 2013, pp. 1–13.

[13] Z. Dong, F. Li, B. Beheshti, A. Mickelson, M. Panero, and N. Anid, "Autonomous real-time water quality sensing as an alternative to conventional monitoring to improve the detection of food, energy, and water indicators," *J. Environ. Stud. Sci.*, vol. 6, no. 1, pp. 200–207, 2016.

[14] E. N. Ivanov, M. E. Tobar, and R. A. Woode, "Microwave interferometry: Application to precision measurements and noise reduction techniques," *IEEE Trans. Ultrason., Ferroelect., Freq. Control*, vol. 45, no. 6, pp. 1526–1536, Nov. 1998.

[15] S. Kim and C. Nguyen, "A displacement measurement technique using millimeter-wave interferometry," *IEEE Trans. Microw. Theory Techn.*, vol. 51, no. 6, pp. 1724–1728, Jun. 2003.

[16] Y. Yang, H. Zhang, J. Zhu, G. Wang, T.-R. Tzeng, X. Xuan, K. Huang, and P. Wang, "Distinguishing the viability of a single yeast cell with an ultra-sensitive radio frequency sensor," *Lab Chip*, vol. 10, no. 5, pp. 553–555, 2010.

[17] M. Schueler, C. Mandel, M. Puentes, and R. Jakoby, "Metamaterial inspired microwave sensors," *IEEE Microw. Mag.*, vol. 13, no. 2, pp. 57–68, Mar. 2012.

[18] M. T. Jilani, M. Z. Rehman, A. M. Khan, M. T. Khan, and S. M. Ali, "A brief review of measuring techniques for characterization of dielectric materials," *Int. J. Inf. Elect. Eng.*, vol. 1, no. 1, pp. 1–5, Dec. 2012.

[19] R. Mirzavand, M. M. Honari, B. Laribi, B. Khorshidi, M. Sadrzadeh, and P. Mousavi, "An unpowered sensor node for real-time water quality assessment (humic acid detection)," *Electronics*, vol. 7, no. 10, p. 231, 2018.

[20] A. A. Helmy, S. Kabiri, M. M. Bajestan, and K. Entesari, "Complex permittivity detection of organic chemicals and mixtures using a 0.5–3-GHz miniaturized spectroscopy system," *IEEE Trans. Microw. Theory Techn.*, vol. 61, no. 12, pp. 4646–4659, Dec. 2013.

[21] *Basics of Measuring the Dielectric Properties of Materials*, Agilent Technol., Santa Clara, CA, USA, 2005, pp. 1–32.

[22] N. T. Cherpak, A. A. Barannik, Y. V. Prokopenko, T. A. Smirnova, and Y. F. Filipov, "A new technique of dielectric characterization of liquids," in *Nonlinear Dielectric Phenomena in Complex Liquids*. Amsterdam, The Netherlands: Springer, 2005.

[23] P. A. Bernard and J. M. Gautray, "Measurement of dielectric constant using a microstrip ring resonator," *IEEE Trans. Microw. Theory Techn.*, vol. 39, no. 3, pp. 592–595, Mar. 1991.

[24] A. Cataldo, E. De Benedetto, and G. Cannazza, "Quantitative and qualitative characterization of liquid materials," in *Broadband Reflectometry for Enhanced Diagnostics and Monitoring Applications*. Berlin, Germany: Springer, 2011, pp. 51–83.

[25] J. A. Byford, K. Y. Park, and P. Chahal, "Metamaterial inspired periodic structure used for microfluidic sensing," in *Proc. 65th Electron. Compon. Technol. Conf.*, May 2015, pp. 1997–2002.

[26] W. Withayachumnankul, K. Jaruwongrungsee, C. Fumeaux, and D. Abbott, "Metamaterial-inspired multichannel thin-film sensor," *IEEE Sensors J.*, vol. 12, no. 5, pp. 1455–1458, May 2012.

[27] *United States Environmental Protection Agency*. Accessed: May 30, 2019. [Online]. Available: https://www.epa.gov/ground-water-and-drinking-water/national-primary-drinking-water-regulations

[28] *Public Water Systems. 10 NYCRR Part 5-1.52*, Dept. Health, New York, NY, USA, 2018.

[29] *Water Quality Standards for pH, Dissolved Oxygen, Dissolved Solids, Odor, Color and Turbidity. 6 NYCRR Part 703.3*, Dept. Environ. Conservation, New York, NY, USA, 2018.

[30] *National Primary Drinking Water Standards. Control of Lead and Copper. 40 CFR 141 Subpart I*, Environ. Protection Agency, Washington, DC, USA, 2007.

[31] A. Bayram, A. Uzlu, M. Kankal, and T. Dede, "Modeling stream dissolved oxygen concentration using teaching–learning based optimization algorithm," *Environ. Earth Sci.*, vol. 73, no. 10, pp. 6565–6576, May 2015.

[32] J. S. Ramsdell, D. M. Anderson, and P. M. Glibert, "HARRNESS: Harmful algal research and response: A national environmental science strategy 2005–2015," Ecological Soc. Amer., Washington, DC, USA, Tech. Rep. 2005-2015, 2005.

[33] Clean Water Team (CWT), "The clean water team guidance compendium for watershed monitoring and assessment, version 2.0. division of water quality," Elect. Conductivity/Salinity Fact Sheet, FS3.1.3.0(EC), California State Water Resour. Control Board (SWRCB), Sacramento, CA, USA, Tech. Rep. 3.6.1, 2004.

[34] J. B. Pendry, A. J. Holden, D. J. Robbins, and W. J. Stewart, "Magnetism from conductors and enhanced nonlinear phenomena," *IEEE Trans. Microw. Theory Techn.*, vol. 47, no. 11, pp. 2075–2084, Nov. 1999.

[35] F. Falcone, T. Lopetegi, J. D. Baena, R. Marqués, F. Martín, and M. Sorolla, "Effective negative-ε stopband microstrip lines based on complementary split ring resonators," *IEEE Microw. Wireless Compon. Lett.*, vol. 14, no. 6, pp. 280–282, Jun. 2004.

[36] H.-J. Lee, H.-S. Lee, K.-H. Yoo, and J.-G. Yook, "DNA sensing using split-ring resonator alone at microwave regime," *J. Appl. Phys.*, vol. 108, no. 1, 2010, Art. no. 014908.

[37] M. S. Boybay and O. M. Ramahi, "Non-destructive thickness measurement using quasi-static resonators," *IEEE Microw. Wireless Compon. Lett.*, vol. 23, no. 4, pp. 217–219, Apr. 2013.

[38] M. S. Boybay and O. M. Ramahi, "Material characterization using complementary split-ring resonators," *IEEE Trans. Instrum. Meas.*, vol. 61, no. 11, pp. 3039–3046, Nov. 2012.

[39] C.-S. Lee and C.-L. Yang, "Thickness and permittivity measurement in multi-layered dielectric structures using complementary split-ring resonators," *IEEE Sensors J.*, vol. 14, no. 3, pp. 695–700, Mar. 2014.

[40] C.-S. Lee and C.-L. Yang, "Complementary split-ring resonators for measuring dielectric constants and loss tangents," *IEEE Microw. Wireless Compon. Lett.*, vol. 24, no. 8, pp. 563–565, Aug. 2014.

[41] M. A. H. Ansari, A. K. Jha, and M. J. Akhtar, "Design and application of the CSRR-based planar sensor for noninvasive measurement of complex permittivity," *IEEE Sensors J.*, vol. 15, no. 12, pp. 7181–7189, Dec. 2015.

[42] *Altair FEKO*. Accessed: May 30, 2019. [Online]. Available: https://altairhyperworks.com/product/FEKO

[43] G. Gennarelli, S. Romeo, M. R. Scarfi, and F. Soldovieri, "A microwave resonant sensor for concentration measurements of liquid solutions," *IEEE Sensors J.*, vol. 13, no. 5, pp. 1857–1864, May 2013.

[44] M. H. Zarifi, M. Fayaz, J. Goldthorp, M. Abdolrazzaghi, Z. Hashisho, and M. Daneshmand, "Microbead-assisted high resolution microwave planar ring resonator for organic-vapor sensing," *Appl. Phys. Lett.*, vol. 106, Jan. 2015, Art. no. 062903.

[45] N. Suwan, "Investigation of RF direct detection architecture circuits for metamaterial sensor applications," M.S. thesis, Dept. Elect. Comput. Eng., Univ. Waterloo, Waterloo, ON, Canada, 2011.

[46] S. Okamura, Y. Zhang, and N. Tsukamoto, "A new microstripline-type moisture sensor for heavily wet tea leaves," *Meas. Sci. Technol.*, vol. 18, no. 4, pp. 1022–1028, 2007.

[47] Z. Meng and Z. Li, "RFID tag as a sensor—A review on the innovative designs and applications," *Meas. Sci. Rev.*, vol. 16, no. 6, pp. 305–315, 2016.

[48] P. Kalansuriya, N. C. Karmakar, and E. Viterbo, "On the detection of frequency-spectra-based chipless RFID using UWB impulsed interrogation," *IEEE Trans. Microw. Theory Techn.*, vol. 60, no. 12, pp. 4187–4197, Dec. 2012.

REZA K. AMINEH received the Ph.D. degree in electrical engineering from McMaster University, Canada, in 2010. He was a Principal Scientist with the Department of Sensor Physics, Halliburton Co. He was a Postdoctoral Fellow with the University of Toronto and McMaster University, from 2012 to 2013 and from 2010 to 2012, respectively. He was a Ph.D. Intern with the Advanced Technology Group, BlackBerry, in 2009. He is currently an Assistant Professor with the Department of Electrical and Computer Engineering, New York Institute of Technology (NYIT). He has authored/coauthored over 65 journal and conference papers, and two book chapters. He contributed to more than 40 patent disclosures in applied electromagnetics while working at Halliburton Co and received several industrial awards. His research interests include applied electromagnetics with applications in imaging and sensing, antennas and microwave components design, and nondestructive testing among the others. He was a recipient of the Banting Postdoctoral Fellowship from the Government of Canada, in 2012, and the Ontario Ministry of Research and Innovation (OMRI) Postdoctoral Fellowship, in 2010. During his Ph.D. program, he received the McMaster Internal Prestige Scholarship Clifton W. Sherman for two consecutive years. He has coauthored an Honorable Mention Paper presented at the IEEE Symposium on Antennas and Propagation, and the International Union of Radio Science, in 2008. He has also coauthored a paper selected among the journal of Inverse Problems *Highlights Collection of 2010*.
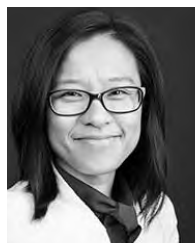
ZIQIAN DONG received the M.S. and Ph.D. degrees in electrical engineering from the New Jersey Institute of Technology. She is currently an Associate Professor with the Department of Electrical and Computer Engineering, New York Institute of Technology (NYIT). Her research interests include architecture design and analysis of high-performance packet switches, data center networks, network security and forensics, wireless sensor networks, and assistive medical devices. She serves as a Faculty Mentor for the Society of Women Engineer NYIT student chapter. She is a Senior Member of the IEEE Communications Society, IEEE Women in Engineering, and a member of the American Society for Engineering Education (ASEE), ACM, and the Environmental Sensing, Networking and Decision-Making (ESND) technical committee. She has served in the Technical Program Committee of IEEE GLOBECOM, ICC, HPSR, Sarnoff, GREENCOM, and as a Reviewer for IEEE journals, conferences, and NSF panels. She was a recipient of the 2006 and 2007 Hashimoto Fellowship for outstanding scholarship, the New Jersey Inventors Hall of Fame Graduate Student Award for her inventions in network switches, and the NYIT Presidential Engagement Award in Student Engagement in Research and Scholarship. She received the Hashimoto Prize for the best Ph.D. dissertation in electrical engineering, NJIT.

KUNYI ZHANG received the B.Sc. degree from Xidian University, Xi'an, China, in 2016, and the M.Sc. degree from the Department of Electrical and Computer Engineering (ECE), New York Institute of Technology (NYIT), in 2018, where he is currently a Research Assistant working on microwave sensing of water/soil quality. He has coauthored a paper titled A microwave sensor array for water quality testing that was selected as a finalist in student paper competition at 20th annual IEEE Wireless and Microwave Technology Conference (WAMI-CON). His research interests include RFID, microwave sensing, microwave measurements, and water/soil quality testing using cost-effective and compact microwave sensor systems.

DAVID NADLER received the Ph.D. degree in health science from Touro University, in 2013, conducted research that modeled allergy development to prenatal antibiotic exposure. He has joined the New York Institute of Technology (NYIT) after a long tenure as a Director with the New York City Department of Environmental Protection. An alumni of the program and an adjunct faculty member, he joined NYIT as the Chair of the Department of the Environmental Technology and Sustainability, in 2017. His test of the hygiene hypothesis can be applied to any environmental systems. By applying his backgrounds in health science and environmental technology, he focuses on making the Environmental Technology and Sustainability degree truly interdisciplinary. He is focused on showing how proper environmental infrastructure improves the quality of life and health for society. He serves as a Reviewer for the *Journal of Bioremediation*.

• • •